# INVESTIGATION ON ALUMINUM-BASED AMORPHOUS METALLIC GLASS AS NEW ANODE MATERIAL IN LITHIUM ION BATTERIES

Shirley Y. Meng[1], Li Yi[1,2] and G. Ceder[1,3]

1. Singapore-MIT Alliance, Advanced Materials for Micro- and Nano- Systems Programme, Engineering Drive, Singapore 117576

2. Department of Materials Science, National University of Singapore, Lower Kent Ridge, Singapore119260

3. Department of Materials Science and Engineering, Massachusetts Institute of Technology, Cambridge, MA 02139

*Abstract*—**Aluminum based amorphous metallic glass powders were produced and tested as the anode materials for the lithium ion rechargeable batteries. Ground $Al_{80}Ni_{10}La_{10}$ was found to have a low first cycle capacity of about 100 Ah/Kg. The considerable amount of intermetallic formed in the amorphous glass makes the aluminum inactive towards the lithium. The ball milled $Al_{88}Ni_9Y_3$ powders contain pure aluminum crystalline particles in the amorphous matrix and have first cycle capacity of about 500 Ah/Kg. Nevertheless, polarization was caused by oxidation introduced by the ball-milling process. The electrochemical performances of these amorphous metallic glasses need to be further investigated. Their full lithium insertion capacities cannot be confirmed until the compositions and particle size inside the metallic glass anodes, the conformation of the electrodes and the mechanical milling processes are optimized.**

***Index Terms*— amorphous metallic glass, lithium ion batteries**

## I. INTRODUCTION

Lithium ion batteries have been the key power source for portable electronics, offering high specific energy, excellent cyclability and flexible design. Graphite has been widely used as anode material for lithium ion batteries; however, its theoretical specific capacity is limited to 372 Ah/Kg[1, 2]. The announcement of the development of lithium batteries containing tin-based composite oxide (TCO) has caused a renewed interest in lithium alloys as alternative materials for the use as anode in rechargeable lithium batteries [3]. Although they can have reversible capacity higher than commercial anode material, the first cycle irreversible capacity required to convert the oxides to alloys is a significant handicap to their introduction[3, 4].

Metallic alloys have a potential anodic capacity of 1000-2000 Ah/Kg[5, 6], but their cycle life is limited due to large volume changes upon discharging/charging. Numerous attempts have been made to stabilize the morphology of alloy based electrodes by minimizing/ buffering the stress in the electrode caused by the volume change[3, 7, 8]. In TCOs, a nano-structure active phase is dispersed in a matrix formed on the initial charge. This amorphous matrix is believed to have a cushioning effect on the stress developed.

We have investigated the use of the aluminum based amorphous metallic glasses $Al_{88}Ni_9Y_3$ and $Al_{80}Ni_{10}La_{10,}$ as the anode in lithium ion rechargeable cells. Amorphous metallic glasses have no long-range ordered microstructure; the atoms are less closely packed compared to the crystalline alloys of the same composition[9, 10]. They usually have higher ionic conductivity than crystalline materials, which may make fast lithium diffusion possible.

## II. EXPERIMENTAL

One of the main challenges is to produce fine powders of amorphous metallic glass in the range of a few micron meters. We are able to obtain ribbons consist of nano-crystalline α-Al dispersed in the amorphous metallic glass matrix. We then mechanically milled the ribbons into powders, while trying to retain their original microstructure.

### *A. Production of Amorphous Metallic Glass*

The aluminum shots (Aldrich 5-15mm 99.9%), nickel spheres (Aldrich 6-16mm 99.95%) and yttrium ingots (Aldrich 99.9%) /lanthanum ingots (Aldrich 99.9%) were arc-melted and homogeneously mixed under argon atmosphere according to the nominal compositions of 88:9:3 and 80:10:10 (atomic percentage) respectively. The alloy was then rapidly solidified into form of ribbons by melt spinning. This was carried out in argon atmosphere using a copper wheel with a typical circumferential velocity of 30m/s. The melt-spun ribbons were typically about 20 μm thick, 1 to 2 mm wide, and up to several meters long.

The microstructures of the melt-spun ribbons were analyzed using a TA instrument differential scanning calorimeter (DSC), a Philip x-ray diffractometer with a Cu $K_\alpha$ x-ray radiation and a JEOL JEM-100CXII transmission electron microscope (TEM) operating at 100kV.

*B. Electrode Preparation*

The melt-spun $Al_{80}Ni_{10}La_{10}$ ribbons were brittle and were hand-ground into powders using mortar and pestle for 30 minutes. The melt-spun $Al_{88}Ni_9Y_3$ ribbons were ductile and had to be milled into powders using Spex8000 high-energy mixer. To minimize the amount of crystallization by avoiding excessive temperature raise, each milling step is 30 or 45 minutes, following by 2 hours resting. The powders were sieved by standard ASTM Mesh325.

The morphology and microstructure of the powders were examined by a JEOL FEG-SEM and a Rigaku RU300 x-ray diffractometer with a Cu $K_\alpha$ x-ray radiation.

Slurries were prepared by mixing the respective powders (95%wt) and polyvinylidene fluoride (PVDF) (5%wt) in acetone. After drying the mixtures they were formed into 5mm diameter pellets.

*C. Electrochemical Testing*

Swagelok-type test cells were assembled using these pellets as the positive electrode, Celgard 2500 micro porous polyethylene membrane as the separator and a 0.75mm thick lithium foil as the negative electrode. The electrolyte was 1.0 M LiPF6 in ethylene carbonate (EC): dimethylcarbonate (DMC) by volume ratio 1:1. Cells were assembled in an argon-filled glove box, where the moisture level is less than 1ppm. All cells were tested using a Maccor 2200 series battery tester.

*D. Characterization of Electrode afterLlithination*

To charcterize the electrode after lithiation, the cell was disassembled in the glove box and the electrode was capped in a special x-ray sample holder in which the electrode could be sealed against air with a layer of x-ray transparent polyimide film. *Ex situ* x-ray characeterization was performed using a Rigaku RU300 x-ray diffractometer with a Cu $K_\alpha$ x-ray radiation.

## III. Results and Discussion

*A. Characterization of Amorphous Metallic Glass Ribbons & Powders*

The DSC results in Figure 1 show that $Al_{80}Ni_{10}La_{10}$ and $Al_{88}Ni_9Y_3$ have major crystallization temperatures $T_x$ at 630K and 627K respectively, indicating good thermal stability of these metallic glasses. $Al_{88}Ni_9Y_3$ has more amorphous phase than $Al_{88}Ni_9Y_3$ because of larger enthalpy of crystallization measure in $Al_{88}Ni_9Y_3$.

The broad maxima in the x-ray diffraction (XRD) spectra of $Al_{80}Ni_{10}La_{10}$ and $Al_{88}Ni_9Y_3$ (Figure 2) confirm that there is amorphous phase in both samples, again the smaller hump of $Al_{80}Ni_{10}La_{10}$ spectrum shows that the amount of amorphous phase in it is less than that in $Al_{88}Ni_9Y_3$. There is a small amount of αAl crystalline phase formed in $Al_{88}Ni_9Y_3$, and the crystalline particles are very fine indicated by broadened peaks in x-ray spectrum. Applying Warren's method [11] of particle size measurement, we calculated that the average particle /crystal size in the glass $Al_{88}Ni_9Y_3$ is about 12.6nm.

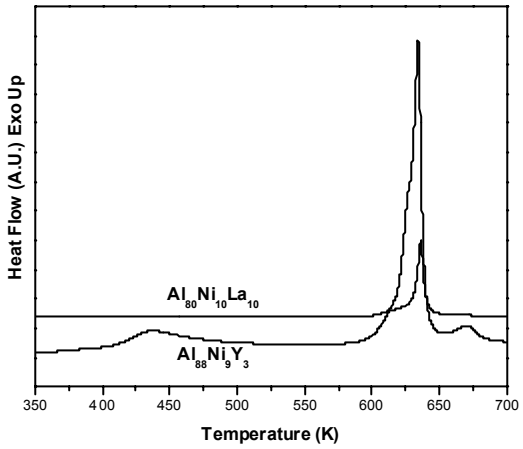


Figure 1. Differential scanning calorimetric curves of melt-spun $Al_{88}Ni_9Y_3$ and $Al_{80}Ni_{10}La_{10}$ ribbons

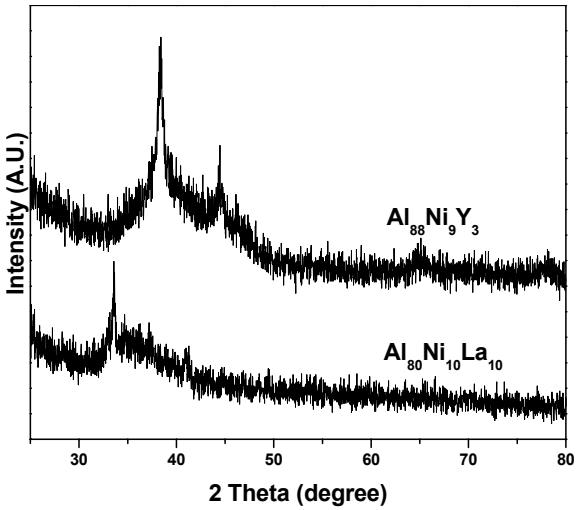


Figure 2. X-ray diffraction spectra of melt-spun $Al_{88}Ni_9Y_3$ and $Al_{80}Ni_{10}La_{10}$ ribbons

Dark field transmission electron microscopy was performed to examine the morphology of the crystalline phase and identify the phases. TEM micrographs Figure 3 (a) and (b) shows that the particle size of the crystalline phase in Al88Ni9Y3 is indeed in the nano-meter range and are dispersed in an amorphous matrix. From Figure 4 (a), it is clear that the crystalline phase in $Al_{80}Ni_{10}La_{10}$ has coarse grains. The selected area electron diffraction (SAED) pattern shown in Figure 4 (b) allows the identification of the crystalline phase as $La_3Al_{11}$.

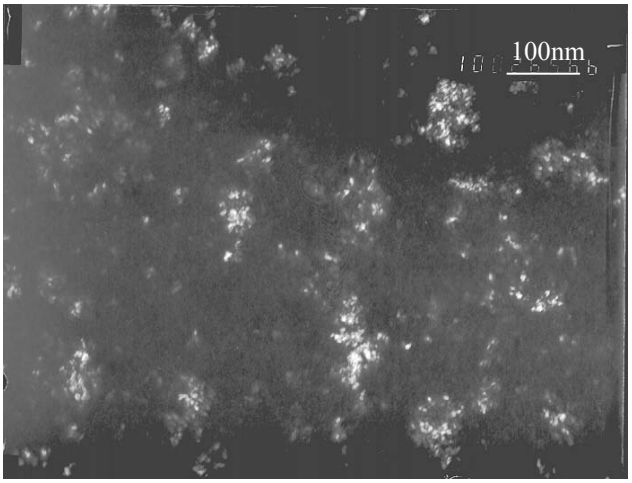


Figure 3 (a)

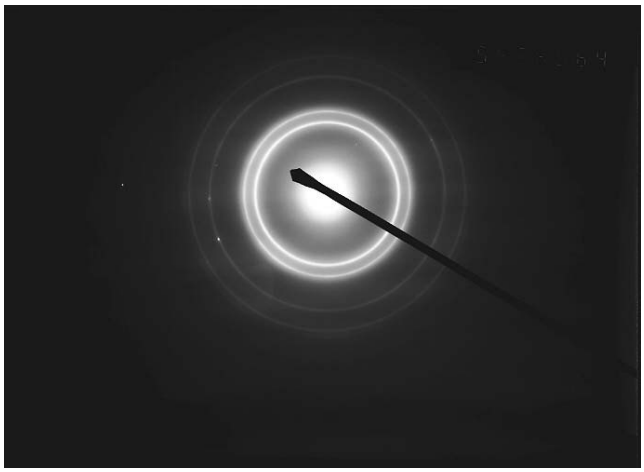

Figure 3 (b)

Figure 3. (a) Dark-field image (b) Electron diffraction pattern, showing the as-quenched structure of $Al_{88}Ni_9Y_3$ ribbons produced at a roller rotation speed 30m/s.

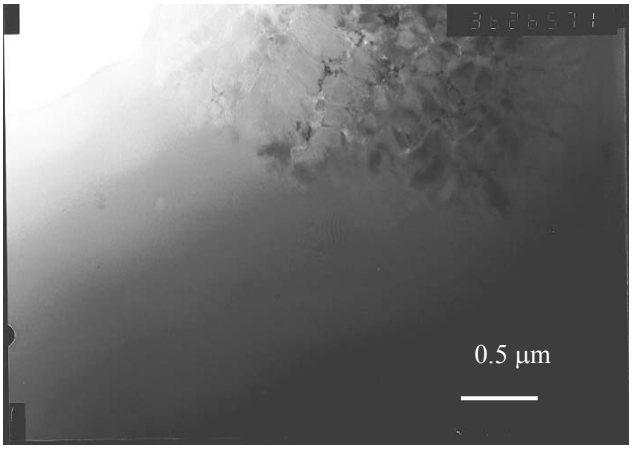


Figure 4 (a)

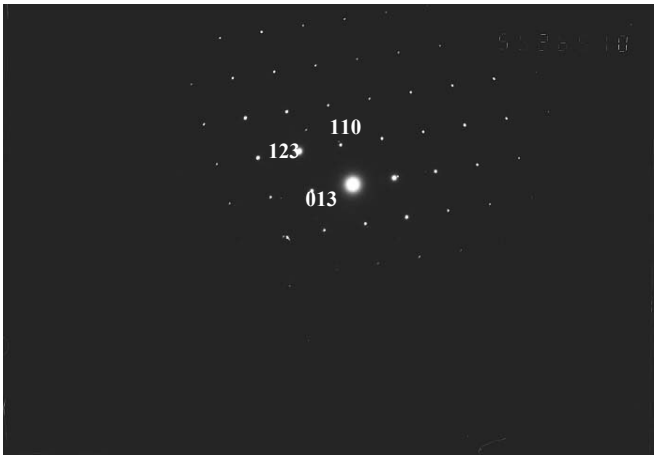


Figure 4 (b)

Figure 4 (a) Dark-field image (b) Electron diffraction pattern, showing the as-quenched structure of $Al_{80}Ni_{10}La_{10}$ ribbons produced at a roller rotation speed 30m/s.

The sieved ball milled $Al_{88}Ni_9Y_3$ have average particle size about 20μm, though there are some larger particles (maximum 40 μm). The particles have irregular morphology and have larger amount of surface area compared with spherical pure aluminum powders (shown in Figure 5 (a) & (b)).

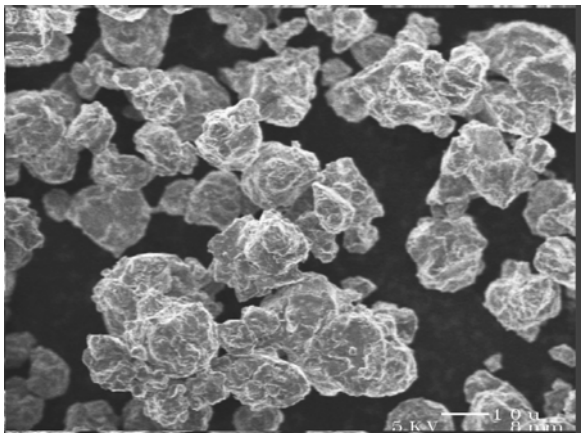

Figure 5 (a)

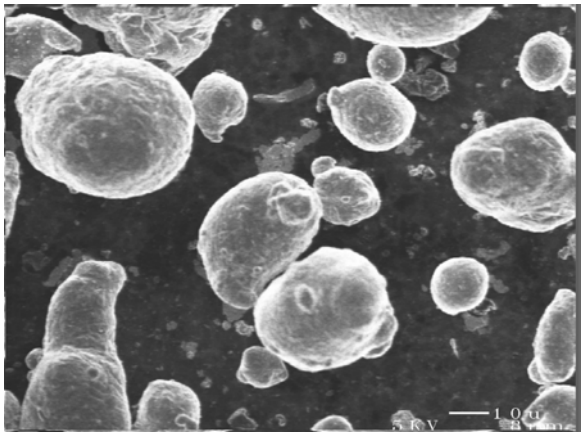

Figure 5 (b)

Figure 5. Scanning electron micrographs showing the powder morphology of (a) sieved ball milled $Al_{88}Ni_9Y_3$ powders and (b) pure aluminum powders (average size - 20μm)

About 30% of the amorphous phase in $Al_{88}Ni_9Y_3$ was crystallized during ball milling, as indicated by comparing the enthalpies of crystallization in the DSC curves (Figure 6) of the as-spun ribbon and the milled powders. Identification of the crystalline phase was again done by x-ray diffraction; the peaks are labeled in Figure 7 (a). It is clear that the amount of nano-sized αAl has increased; yet the particle size has not grown significantly. In the ground $Al_{80}Ni_{10}La_{10}$ powders XRD spectrum shown in Figure 7 (b), a large amount of intermetallic $La_3Al_{11}$ phase was precipitated from amorphous matrix.

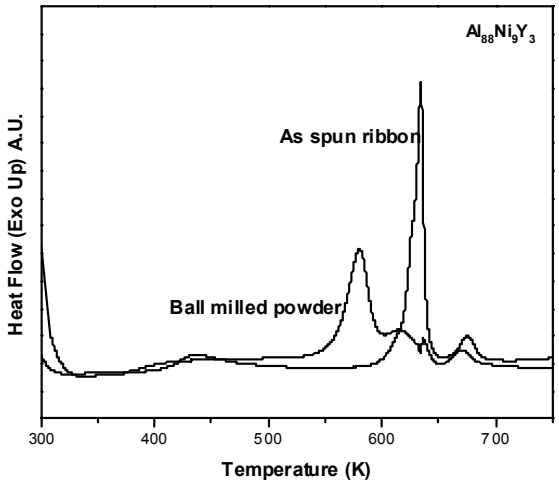


Figure 6. Differential scanning calorimetric curves of melt-spun $Al_{88}Ni_9Y_3$ ribbon and ball milled powder.

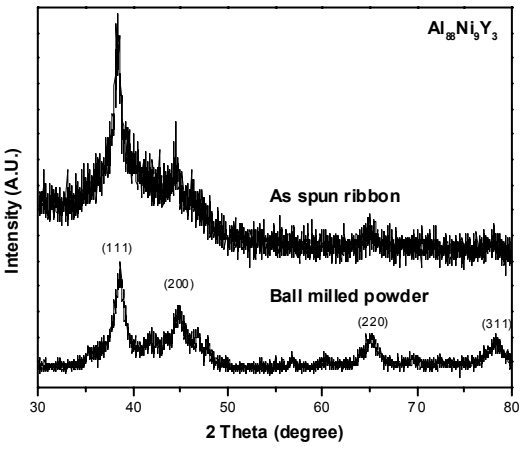


Figure 7 (a)

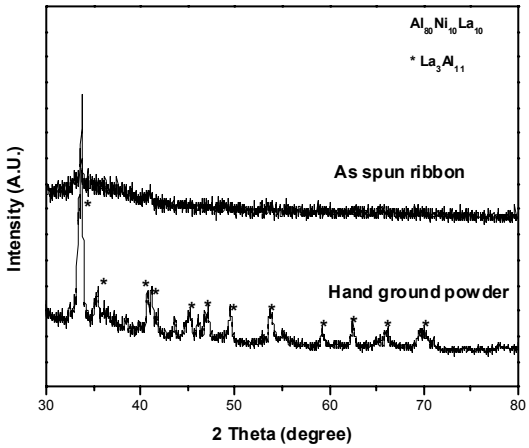


Figure 7 (b)

Figure 7. X-ray diffraction spectra of (a) melt-spun $Al_{88}Ni_9Y_3$ ribbon and hand ground powder; (b) melt-spun $Al_{80}Ni_{10}La_{10}$ ribbon and hand ground powder.

*B. Electrochemical Testing*

*1) Ground $Al_{80}Ni_{10}La_{10}$ Powders*

Electrodes made from ground $Al_{80}Ni_{10}La_{10}$ powders were cycled at 40μA from 3V to 0V and 100μA from 3V to 0V. Figures 8 (a) and (b) show the respective charge and discharge curves under those conditions. The lithium insertion voltage of the aluminum based metallic glass is about 0.2 Volt, lower than that of pure aluminum: V=0.30 Volt [12]. The polarization probably comes from the grinding process; grinding process seems to cause a decrease in the electronic conductivity of the electrode, as has been suggested for other ground powders [13]. Nickel and yttrium do not react with lithium at room temperature. If it is assumed that only the aluminum in the amorphous glass reacts to form LiAl (this is confirmed by XRD result shown in the next section), the theoretical capacity should be about 560Ah/Kg. The capacity obtained is about 100 Ah/Kg for 40μA; the low capacity is consistent with the microstructure analysis as a large amount of aluminum was 'locked' by the intermetallic $La_3Al_{11}$. There is further decrease in capacity when we cycled the cells at 100μA, refer to Figure 8 (c).

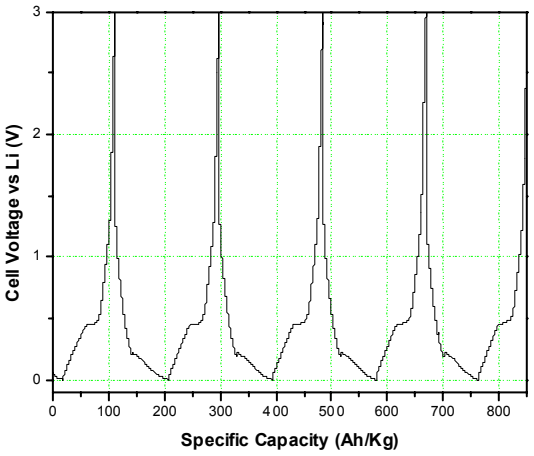


Figure 8 (a)

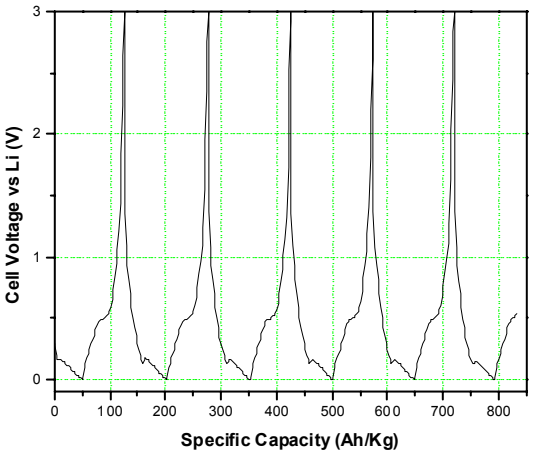


Figure 8 (b)

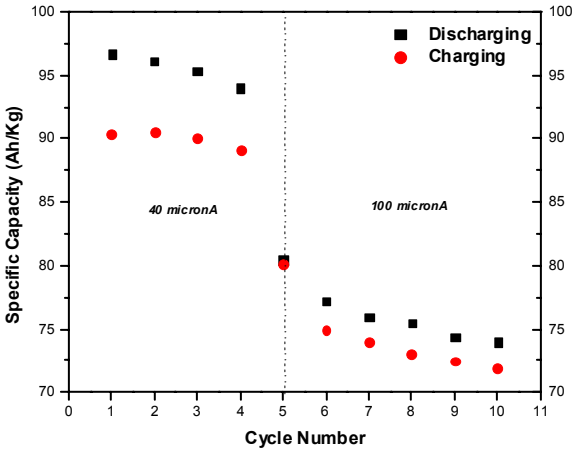


Figure 8 (c)

Figure 8. (a) Cycling of electrochemical Li insertion and release on $Al_{80}Ni_{10}La_{10}$ at constant current of 0.04mA per 10.2mg $Al_{80}Ni_{10}La_{10,}$ conducted at room temperature between voltage limits of 0V and 3V (C/170). (b) Cycling of electrochemical Li insertion and release on $Al_{80}Ni_{10}La_{10}$ at constant current of 0.04mA per 10 mg $Al_{80}Ni_{10}La_{10,}$ conducted at room temperature between voltage limits of 0V and 3V (C/70). (c) Cycle performance with different C-rates.

*2) Ball Milled $Al_{88}Ni_9Y_3$ Powders*

As it is shown in the first discharge-charge cycle (Figure 9 (a)), the lithium insertion voltage for the ball milled $Al_{88}Ni_9Y_3$ powders was lowered further down to 0.03V, which was most possibly caused by the high-energy ball milling process. Applying the same assumption above, the theoretical capacity of $Al_{88}Ni_9Y_3$ is approximately 750Ah/Kg. The first discharge and charge capacity are 496Ah/Kg and 340Ah/Kg, respectively. Large capacity loss was observed in subsequent cycles, shown in Figure 9 (b).

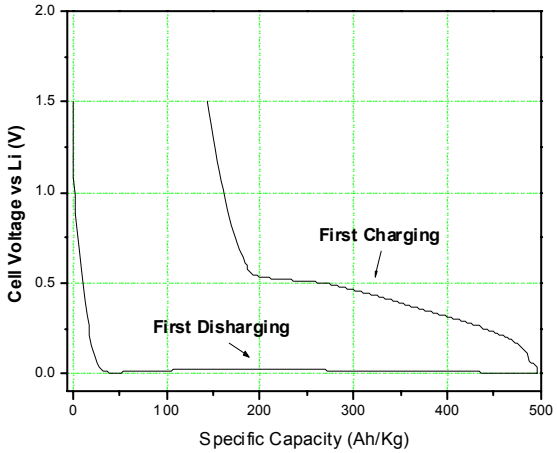


Figure 9 (a)

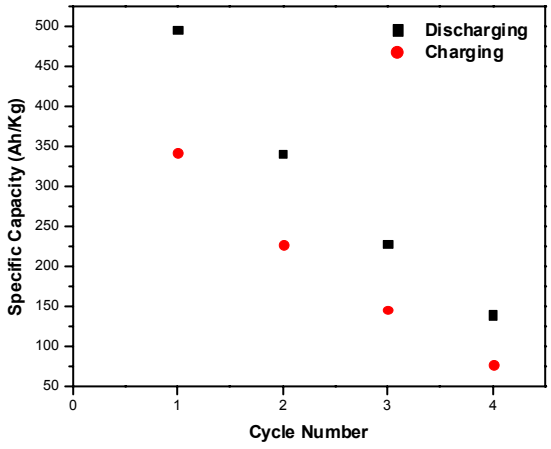


Figure 9 (b)

Figure 9. (a) First discharge-charge cycle (b) Cycle performance of electrochemical Li insertion and release on $Al_{88}Ni_9Y_3$ at constant current of 0.03mA per 7.2mg $Al_{88}Ni_9Y_3$, conducted at room temperature between voltage limits of 0V and 1.5V (C/180).

It is suspected that during the ball milling, air leaked into the ball milling vial. Since aluminum is extremely susceptible to oxygen, the electrode material contains a certain amount of oxides, which explains why the polarization is severe and the irreversible capacity is large. The oxidation also caused the lithium insertion process hindered by kinetics; the cells could only be cycled as very low rate such at C/180 in this work.

### *C. Characterization of Lithium Inserted Electrodes*

X-ray diffraction was carried out to detect the phase formed after the first cycle lithium insertion in $Al_{88}Ni_9Y_3$ electrode. The background caused by the polyimide film that covered the electrode was subtracted. It can be seen from Figure 10 that LiAl formed in the electrode after discharging the cell.

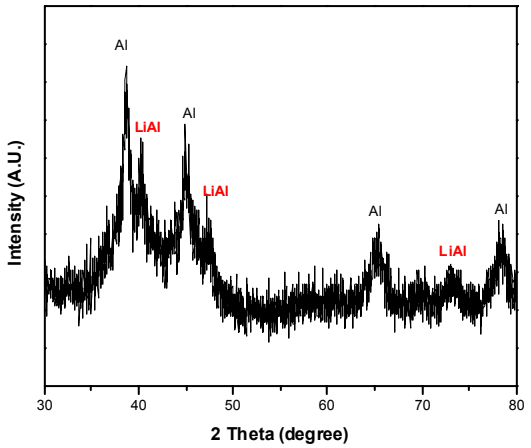


Figure 10. X-ray diffraction spectrum of the lithium inserted $Al_{88}Ni_9Y_3$ electrode.

## IV. CONCLUSIONS

Aluminum based amorphous metallic glass powders were produced and tested as the anode materials for the lithium ion rechargeable batteries. Ground $Al_{80}Ni_{10}La_{10}$ was found to have a low first cycle capacity of about 100 Ah/Kg. The considerable amount of intermetallic formed in the amorphous glass makes the aluminum inactive towards the lithium. The ball milled $Al_{88}Ni_9Y_3$ powders contain pure aluminum crystalline particles in the amorphous matrix and have first cycle capacity of about 500 Ah/Kg. Nevertheless, polarization was caused by oxidation introduced by the ball milling process. The inadequate electrochemical characteristics we obtained are not conclusive. The electrochemical performances of these amorphous metallic glasses need to be further investigated. Their full lithium insertion capacities cannot be confirmed until the compositions and particle size inside the metallic glass anodes, the conformation of the electrodes and the ball milling conditions are optimized.

## ACKNOWLEDGMENT

This work has been funded by the Singapore-MIT Alliance, National University of Singapore. We also acknowledge the discussions with Dr. M. E. Arroyo (Massachusetts Institute of Technology), who provided helpful ideas in this work.

## REFERENCES

1.Takehara, Z. and K. Kanamura, *Historical Development of Rechargeable Lithium Batteries in Japan.* Electrochimica Acta, 1993. **38**(9): p. 1169-1177.

2.Tarascon, J.M. and M. Armand, *Issues and challenges facing rechargeable lithium batteries.* Nature, 2001. **414**(6861): p. 359-367.

3.Idota, Y., et al., *Tin-based amorphous oxide: A high-capacity lithium-ion-storage material.* Science, 1997. **276**(5317): p. 1395-1397.

4.Huggins, R.A., *Lithium alloy negative electrodes formed from convertible oxides.* Solid State Ionics, 1998. **115**: p. 57-67.

5.Fauteux, D. and R. Koksbang, *Rechargeable Lithium Battery Anodes - Alternatives to Metallic Lithium.* Journal of Applied Electrochemistry, 1993. **23**(1): p. 1-10.

6.Huggins, R.A., *Lithium alloy negative electrodes.* Journal of Power Sources, 1999. **82**: p. 13-19.

7.Kepler, K.D., J.T. Vaughey, and M.M. Thackeray, *Copper-tin anodes for rechargeable lithium batteries: an example of the matrix effect in an intermetallic system.* Journal of Power Sources, 1999. **82**: p. 383-387.

8.Thackeray, M.M., J.T. Vaughey, and C.S. Johnson, *Recent advances in electrode materials for lithium batteries.* Abstracts of Papers of the American Chemical Society, 2001. **221**: p. 609-INOR.

9.He, Y., S.J. Poon, and G.J. Shiflet, *Synthesis and Properties of Metallic Glasses That Contain Aluminum*, in *Science*. 1988. p. 1640-1642.

10.Inoue, A., *Amorphous, nanoquasicrystalline and nanocrystalline alloys in Al-based systems.* Progress in Materials Science, 1998. **43**(5): p. 365-520.

11.Cullity, B.D., *Elements of X-ray Diffraction*. 2001, Upper Saddle River, NJ: Prentice Hall.

12.Meng Ying, L.Y., E. M. Arroyo and G. Ceder. *Amorphous Metallic Glass as New High Power and Energy Density Anodes For Lithium Ion Rechargeable Batteries*. in

*Singapore-MIT Alliance Annual Symposium 2002*. 2002. Singapore.

13.M. E. Arroyo Y De Dompablo, E.M., A, Varez and F. Garcia-alvarado, *Electrode Characterization of $Li_2Ti_3O7$* - ramsdellite Processed by Mechanical Grinding. Journal of Materials Science, 2002. 37: p. 3981-3986.